Interband and intersubband absorption in HgCdTe multiple quantum wells

A. M. de Paula* and C. R. M. de Oliveira
Instituto de Física, Universidade Estadual de Campinas, Caixa Postal 6165, 13083-970 Campinas-SP, Brazil

G. E. Marques
Departamento de Física, Universidade Federal de São Carlos, 13565-905 São Carlos-SP, Brazil

A. M. Cohen
Departamento de Física, Universidade Federal do Amazonas, 69000 Manaus-AM, Brazil

R. D. Feldman and R. F. Austin
Lucent Technology, Bell Laboratories, Holmdel, New Jersey 07733

M. N. Islam
University of Michigan, Ann Arbor, Michigan 48109

C. L. Cesar
Instituto de Física, Universidade Estadual de Campinas, Caixa Postal 6165, 13083-970 Campinas-SP, Brazil
(Received 19 August 1998)

We present calculated and experimental interband and photoinduced intersubband absorption spectra for undoped HgCdTe multiple quantum wells. The results show that there is an enhancement of the interband absorption at energies close to the barrier energy for electrons. The calculated interband absorption, based on a full 8×8 $\mathbf{k}\cdot\mathbf{p}$ Kane model to obtain the electronic structure, predicts that this absorption enhancement is caused by an increase in the electron-hole joint density of states due to band mixing for confined and continuous electron states. The photoinduced electron intersubband absorption presents an asymmetric line shape due to the nonparabolic bands. The calculated spectra reproduce well the experimental results. [S0163-1829(99)04215-0]

I. INTRODUCTION

The electronic band structure in multiple quantum wells (MQW's) and superlattices are now reasonably understood. Many theoretical and experimental studies have shown details such as confined energy states, excitonic effects, and hole band mixing.[1,2] Also, recently a complete calculation of the bound-to-continuum hole transitions in good agreement with experimental results has been presented for *p*-type quantum wells.[3,4]

The interest in HgCdTe MQW arises because of their potential applications as infrared optical modulators, lasers, detectors, and emitters. In these narrow-gap structures the large nonparabolicity effects and interband mixing, and the small effective masses provide a rich variety of novel optical and electronic properties. Meyer *at al.*[5] presented a recent review of these properties. The experimental and calculated absorption spectra near the band edge describe well the various interband transitions between the confined electron and hole states.[5–8] Nonetheless the interband absorption near the barrier energy is not yet well established. In this paper we present calculated and experimental interband absorption spectra covering the energy range from the band edge to the barrier energy in undoped HgCdTe MQW. The results show that there is an enhancement of the interband absorption at energies close to the barrier energy for electrons. The calculated interband absorption, based on a full 8×8 $\mathbf{k}\cdot\mathbf{p}$ Kane model to obtain the electronic structure, predicts that this interband absorption enhancement is caused by an increase in the electron-hole joint density of states due to band mixing for confined and continuous electron states.

We also present calculated photoinduced electron intersubband absorption showing an asymmetric line shape due to the nonparabolic bands. In a previous paper we presented experimental results for this asymmetric line shape[9] and we simulated the experimental results considering different effective masses for the electron subbands. Now we show the complete calculated photoinduced intersubband spectra that reproduce well the experimental results.[9]

The experimental results for both the interband and intersubband absorption were reproduced with a value of 360 meV for the valence band offset in the band structure calculations. These results corroborate to determine that the offset should be close to 360 meV. A range of 350–400 meV was established in the literature.[5,10]

II. EXPERIMENTAL

We studied two undoped MQW samples grown by molecular beam epitaxy on GaAs substrate with the following layer sequence: a 0.3 μm ZnTe layer, a 2 μm CdTe layer, followed by the 50 period MQW's, consisting of a 100 Å thick $Hg_{0.83}Cd_{0.27}Te$ well or a 80 Å thick $Hg_{0.60}Cd_{0.40}Te$ well separated by a 100 Å thick $Hg_{0.15}Cd_{0.85}Te$ barrier.

The interband absorption measurements were performed using a Mattson Fourier transform spectrometer for the energy region below approximately 650 meV. For the higher energy (580–1400 meV) we used a Cary spectrometer. All spectra were taken with the sample at room temperature. The Fabry-Perot interference fringes were minimized by using a broad band polarizer and positioning the sample at Brewster's angle for the MQW-air interface. We joined the two absorption spectra by matching the overlapping energy region of the measured spectra.

The photoinduced intersubband absorption spectra were taken in a pump and probe configuration. Photoexcited electrons in the first electron subband were generated from a 5 W cw Nd:YAG pump laser. The intersubband transition from the first to the second electron subband were probed by infrared light focused on a sample polished edge at 45° with the growth direction (z). This geometry allowed coupling to the intersubband transition for light polarization in the z direction.[9]

III. THEORY

The optical absorption in heterolayered semiconductor structures has been demonstrated to be a powerful tool to reveal the intrinsic details of its quantized electronic states. The excitation spectra in these structures are mostly dominated by quasilocalized two-dimensional excitons superimposed to plateaulike steps displaying both the general aspects of the joint-density of state function for intersubband transitions and the related effect due to the Coulombic interaction between the carriers. The selection rules, for optically excited transitions, depend on the light polarization and are determined by the spatial symmetry and by the different hybridization of the involved electronic states and appearing in the linear momentum dependence of $E^{s}_{n,j}(\mathbf{k})$, the energy of carriers inside the Brillouin zone. Here, s labels the spin component, n the subband level, and j the carrier type (electron, heavy hole, light hole, and split-off hole). This set of special conditions shows that, some interband optical transitions (valence-to-conduction), which would be strictly ''forbidden'' in bulk semiconductors ($\Delta n=|n_f-n_i|>0$), can be observed in quantum well structures, although they show much weaker intensities (oscillator strengths) as compared to the ''permitted'' ones ($\Delta n=|n_f-n_i|=0$). For example, the selection rule for optical transitions from the $n_i=n$ state in the valence of a QW to the first conduction subband, $n_f=1$, becomes $n=2p$, $p=0,1,2,3,\ldots$.

A. Electronic structure

The conduction and valence band states in this work are calculated by a modified Kane Hamiltonian,[11] where each envelope function component in the four periodic Bloch functions at the Γ point, namely, $|\frac{1}{2},+\frac{1}{2}\rangle$, $|\frac{3}{2},+\frac{3}{2}\rangle$, $|\frac{3}{2},+\frac{1}{2}\rangle$, $|\frac{1}{2},+\frac{1}{2}\rangle$ for conduction, heavy-hole, light-hole, and split-off hole bands, respectively, are obtained from the solutions of $H^{U}\Psi^{U}_{i,j}(\mathbf{k},\rho,z)=E^{U}_{i,j}(\mathbf{k})\Psi^{U}_{i,j}(\mathbf{k},\rho,z)$. The full Hamiltonian which includes the kinetic and strain terms ($H^{U}=H_{\mathbf{k}\cdot\mathbf{p}}+H_{\text{strain}}$) can be written in the Hermitian form as

$$H^{U}=\begin{bmatrix} D_{el} & & & \\ P_1^* & D_{hh} & & \\ P_2^* & L_1^* & D_{lh} & \\ P_3^* & L_2^* & Q_1^* & D_{\text{SO}} \end{bmatrix}+V(z)I, \quad (1)$$

where $V(z)$ represents the set of potential profiles seen by each carrier in the system and I is a 4×4 identity matrix. The terms representing the sum of kinetic and strain coupling energies for carriers can be written as a function of the band parameters for each material, as

$$D_{el}=\left\{E_g^0+E_\nu^c+\left(F_0+\frac{1}{2}\right)k^2+\left[\hat{k}_z\left(F+\frac{1}{2}\right)\hat{k}_z\right]\right\}+\alpha_h^c, \quad (2)$$

$$D_{hh}=D^{+}+(\alpha_h^v-\beta_v), \quad (3)$$

$$D_{lh}=D^{-}+(\alpha_h^v+\beta_v), \quad (4)$$

with

$$D^{\pm}=\left\{-E_\nu^v-\frac{1}{2}(\gamma_1\pm\gamma_2)k^2-\frac{1}{2}[\hat{k}_z(\gamma_1\mp2\gamma_2)\hat{k}_z]\right\}, \quad (5)$$

$$D_{\text{SO}}=-E_\nu^v-\Delta_{\text{SO}}-\frac{1}{2}\gamma_1k^2-\frac{1}{2}[\hat{k}_z(\gamma_1)\hat{k}_z]+\alpha_h^v, \quad (6)$$

$$P_1=-\sqrt{\frac{1}{2}}P_0k, \quad (7)$$

$$P_2=\left[-\sqrt{\frac{2}{3}}\{P_0,\hat{k}_z\}+i\sqrt{\frac{1}{3}}P_0k\right], \quad (8)$$

$$P_3=\left[-\sqrt{\frac{1}{3}}\{P_0,\hat{k}_z\}+i\sqrt{\frac{1}{3}}P_0k\right], \quad (9)$$

$$Q_1=\left[\sqrt{2}[\hat{k}_z\gamma_2\hat{k}_z]-\sqrt{\frac{1}{2}}\gamma_2k^2-i\frac{3}{\sqrt{2}}k\{\gamma_3,\hat{k}_z\}\right]-\sqrt{2}\beta_v, \quad (10)$$

$$L_1=\left[\sqrt{3}k\{\gamma_3,\hat{k}_z\}+i\frac{\sqrt{3}}{2}k^2\gamma(\theta)\right], \quad (11)$$

$$L_2=\left[-\sqrt{\frac{3}{2}}k\{\gamma_3,\hat{k}_z\}+i\sqrt{\frac{3}{2}}k^2\gamma(\theta)\right], \quad (12)$$

where E_g^0 is the energy gap, $E_\nu^{c(v)}$ is the band offset for conduction (valence) band, Δ_{SO} is the spin-orbit energy for the material in the absence of strains, $\hat{k}_z=-i(d/dz)$, θ is the angle between the components (k_x,k_y) and $k=\sqrt{k_x^2+k_y^2}$ is the modulus of the parallel momentum in the xy plane. The brackets indicates the relation $\{a,b\}=ab+ba$. The γ_1, γ_2, γ_3, F_0, and P_0 are the well known Kane parameters for the bulk dispersions of each material. The strain terms α and β are defined in terms of the elastic compliance tensor components, as $\alpha_h^c=-2(S_{xx}+2S_{xy})/(S_{xx}+S_{xy})\epsilon_\perp a_h^c$ and $\alpha_h^v=-2(S_{xx}+2S_{xy})/(S_{xx}+S_{xy})\epsilon_\perp a_h^v$ for hydrostatic strain in the conduction and valence bands, re-

spectively, and the axial deformation as $\beta_v = -(S_{xx} - S_{xy})/(S_{xx} + S_{xy})\epsilon_\perp b_u^v$. The hydrostatic strain changes the gap as $E_g^* = [E_g^0 + (\alpha_h^c - \alpha_h^v)]$, however the axial deformation produces different energy gaps for heavy and light-hole states in the form $E_g^{hh(lh)} = (E_g^* \pm \beta_v)$. Certainly these changes produced by strain will affect the heights of the barriers (band-offset) for each type of carrier.

The overall result of strain effects on the valence band states of layered structures depends on if a given layer is submitted either to an extension or to a compression with respect to substrate. The deformation in the xy plane of a heterolayered system is determined by the percentual mismatch in the lattice parameters $\epsilon_\perp = (a_{\text{layer}} - a_{\text{sub}})/a_{\text{sub}}$, where a_{sub} and a_{layer} stand for the lattice parameter of the substrate and of a given layer, respectively. Thus, $a_{\text{layer}} = a_{\text{sub}}(1 + \epsilon_\perp)$ and one can see that for those layers under compression ($a_{\text{layer}} < a_{\text{sub}}$) the strain in the xy plane is $\epsilon_\perp < 0$ and those under extension ($a_{\text{layer}} > a_{\text{sub}}$) the strain is $\epsilon_\perp > 0$.

The envelope functions which are solutions of Eq. (1) for the ith state in the conduction band, with envelope function components in the Bloch states at the Γ point having only positive spin components $J_z = +\frac{1}{2},\ +\frac{3}{2},\ +\frac{1}{2},\ +\frac{1}{2}$ and labeled U states or having negatives spin components and labeled L states, are written in the form

$$\Psi_{i,c}^U(\mathbf{k},\rho,z) = e^{i\mathbf{k}\cdot\rho}\begin{bmatrix} F_1^{i,c}(\mathbf{k},\rho,z) \\ F_2^{i,c}(\mathbf{k},\rho,z) \\ F_3^{i,c}(\mathbf{k},\rho,z) \\ F_4^{i,c}(\mathbf{k},\rho,z) \end{bmatrix}, \tag{13}$$

$$\Psi_{i,c}^L(\mathbf{k},\rho,z) = e^{i\mathbf{k}\cdot\rho}\begin{bmatrix} F_5^{i,c}(\mathbf{k},\rho,z) \\ F_6^{i,c}(\mathbf{k},\rho,z) \\ F_7^{i,c}(\mathbf{k},\rho,z) \\ F_8^{i,c}(\mathbf{k},\rho,z) \end{bmatrix}, \tag{14}$$

where $(\mathbf{k},\rho)$ are the momentum and spatial coordinates in the xy plane.

The Hamiltonian determining the L states can be obtained by applying the time-reversal operator $\hat{\mathcal{T}} = -i\hat{\mathbf{I}}\hat{\mathcal{C}}\sigma_z$ to the Hamiltonian in Eq. (1) where $\hat{\mathbf{I}}$ is the spatial inversion, $\hat{\mathcal{C}}$ is the complex conjugation, and σ_z is the Pauli matrix operators. If the applied potential profile shows a center of symmetry, both U and L states will have eigenvalues $E_{i,j}^U(\mathbf{k})$ and $E_{i,j}^L(\mathbf{k})$ degenerated, for all $\mathbf{k}$ inside the Brillouin zone.

The full electronic structure is calculated by solving the Schrödinger equation with the Hamiltonian given in Eq. (1). The Kane parameters F_0, P_0, γ_1, γ_2, and γ_3, which appear in the Hamiltonian, are determined from their direct relations to the carrier effective masses, and are derived from each eigenvalue of Eq. (1), after an expansion to second order in k, as

$$\frac{m_0}{m_c}(001) = \left\{ (2F_0 + 1) + \left(\frac{4m_0 P_0^2}{3E_g\hbar^2} \right) \left[1 + \frac{Eg}{2(Eg + \Delta_{\text{SO}})} \right] \right\}, \tag{15}$$

$$\frac{m_0}{m_{hh}}(001) = [\gamma_1 - 2\gamma_2], \tag{16}$$

$$\frac{m_0}{m_{lh}}(001) = \left[(\gamma_1 + 2\gamma_2) + \left(\frac{4m_0 P_0^2}{3E_g\hbar^2} \right) \right], \tag{17}$$

$$\frac{m_0}{m_{\text{SO}}}(001) = \gamma_1 + \frac{2m_0 P_0^2}{3E_g\hbar^2(E_g + \Delta_{\text{SO}})}, \tag{18}$$

and

$$\frac{m_0}{m_{hh}}(111) = [\gamma_1 - 2\gamma_3]. \tag{19}$$

B. Interband optical transitions

By starting from the full calculated electronic structure $\{\Psi_{j,v}^s(\mathbf{k},\rho,z); E_{i,j}^s(\mathbf{k})\}$ for a given quantum well profile, we can calculate any physical property of the system such as the interband (valence to conduction) optical absorption[12]

$$\alpha_{\text{inter}}(\hbar\omega) = \alpha_{ex}(0) + \alpha_0 \sum_{ij} \int \frac{d^2k}{(2\pi)^2} \mathbf{Q}_{ij}(\mathbf{k}) \mathcal{L}[\Delta E_{i,j}(\mathbf{k}); \Gamma_{ij}], \tag{20}$$

where $\alpha_0 = 2\pi e^2/cm_0 L_z$, is a constant determining the scale for optical transitions in the well of width L_z, $\mathcal{L}(x;y)$ is a Lorentzian lineshape function for the optical transitions, Γ_{ij} is the linewidth for transitions from the initial state j, in the valence subband, to the final state i, in the conduction subband, whose energy difference at each value of the k parallel is $\Delta E_{ij}(\mathbf{k})$. Here, the nonparabolicity, the subband mixing and sensitivity of the subband structure on the external and/or internal fields play an important role.

The quantity $\mathbf{Q}_{ij}(\mathbf{k})$, which measures the probability for vertical optical transitions (proportional to the oscillator strength), excited by photons of polarization $\hat{\eta}$ and frequency ω, may be calculated as

$$Q_{ij}(k) = \frac{1}{m_o} |\langle \Psi_{i,c}(\mathbf{k},\rho,z) | \hat{\eta}\cdot\hat{\mathbf{P}} | \Psi_{j,v}(\mathbf{k},\rho,z) \rangle|^2, \tag{21}$$

where we have dropped the spin-component label s, since we will be restricting our interest in this paper to those structures with potential profiles heaving spatial symmetry and the final results is just the added factor of 2 in α_0.

In general, the linewidth for optical transitions are determined from all homogeneous and inhomogeneous scattering mechanisms present in the sample. The direct calculation of Γ_{ij} would require detailed information on growth conditions of each sample and its detailed characterization. However, we will use later this linewidth as an input parameter for the interband absorption in a given sample, according to the observed shape of peaks in experimental lines.

Finally, $\alpha_{ex}(0)$ is the optical absorption due to the presence of excitons where binding energies and wave functions are calculated variationally after assuming a hydrogeniclike s-type wave function for the ground state. The effective

masses used for hh and lh excitons are determined directly from the dispersions of conduction and valence bands. All details of this approach can be found in Ref. 13. We also use the statistical model for excitonic linewidth[14] together with the quasi-two-dimensional correction[15] to the excitonic volume in the quantum wells of width L_z which gives a fairly good approximation for the inhomogeneous line broadening in the excitonic peaks. For materials with zinc blende symmetry where the cubic sublattice has volume a_0^3, this inhomogeneous linewidth for good quality samples, may be estimated as

$$\Gamma_{ij}=\left(\frac{dE_g^{ij}}{dx}\right)\left[\frac{3a_o^3(1-x)x}{8\pi a_{xc}^2 L_z}\right], \tag{22}$$

where $[dE_g^{ij}(x)/dx]$ is the change in the effective band gap between i and j levels in the QW with a concentration x for structures of type $A_{(1-x)}B_xC$, and a_{xc} is the two-dimensional Bohr radius of the exciton inside the quantum well with values in the range 2–5 meV for $1s$ excitons in CdTe quantum wells. For higher levels, we may estimate the biding energies of excitons, to a good approximation, as $E_b(n)=E_b(1)/n^2$.

C. Intersubband optical transitions

Another important optical characterization for these structures is associated with transitions between confined states in the conduction or valence subbands, intersubband transitions and also transitions from the confined states inside quantum wells to the states above the barrier. Here, the number of states in the continuum region plays a very important role in determining both the effective barrier height as well as the quality of the confinement region or interface quality in the heterostructure as well as possible monolayer fluctuations or interdiffusion of material across interfaces. Recently, Szmulowicz and Brown[3,4] presented a complete calculation of the bound-to-continuum absorption in p-type GaAs/AlGaAs quantum wells showing the importance of a true continuum calculation.

We calculate the intersubband (or intraband) optical absorption for photoinduced electrons,[16] with just slight modifications to Eq. (20), as

$$\alpha_{\text{intra}}(\hbar\omega)=\alpha_{cc}^0\sum_{ij}\int\frac{d^2k}{(2\pi)^2}\mathbf{Q}_{ij}(\mathbf{k})\mathcal{L}[\Delta E_{i,j}(\mathbf{k});\Gamma_{ij}], \tag{23}$$

where

$$\alpha_{cc}^0=\left[\frac{8\pi^2e^2N_0}{\omega c\epsilon_0 n_i m_0^2 L_z}\right]. \tag{24}$$

Here, N_0 is the density of photoexcited electrons in each quantum well by the laser of frequency ω in a semiconductor heaving static dielectric constant ϵ_0 and refractive index n_i, respectively, that can be taken as an average between the values for materials in the well and barrier regions of the heterostructure. Also e and m_0 are the charge and free mass of the electron, respectively, c is the speed of light in vacuum, and L_z is the quantum well width. The $\mathbf{Q}_{ij}(\mathbf{k})$ and $\mathcal{L}[\Delta E_{i,j}(\mathbf{k});\Gamma_{ij}]$ were already defined in Sec. III B and the only change needed to the present case is related to the identification of the initial state, confined state in the well layer, and the final state which can be either confined in the quantum well or states in the continuum with energy above the barrier.

The selection rules in these optical transitions are almost entirely determined by the spatial symmetry (parity) of the initial and final states in the heterostructure and by the odd parity of the momentum operator. However, the envelope wave functions play a very important role here in contrast to the interband case discussed Sec. III B, where the symmetry of the periodic part of Bloch states mainly dictates the selection rules.[17] In the next section, we will use the approach presented here to compare the calculated and experimental optical data for HgCdTe multiple quantum wells.

IV. RESULTS AND DISCUSSION

A typical electronic structure for $Hg_{(1-x)}Cd_xTe$-$Hg_{(1-y)}Cd_yTe$ multiple quantum wells at room temperature $T=300$ K is shown in Fig. 1. The chosen sample has ''direct band structure'' where the conduction band has a normal s character. The well width is $L_z=100$ Å, the Cd concentrations are $x=0.27$ in the well layer and $y=0.85$ in the barrier layer.

The full electronic structure was calculated by solving the Schrödinger equation with the Hamiltonian given in Eq. (1) using the parameters obtained from linear interpolation between those listed in Table I, and a valence band offset $E_v^v=360$ meV. The conduction band offset E_v^c is calculated from the energy band gaps $E_g(x,T)$, measured in meV and for values of T above 70 K, which is obtained from a fitting to many experimental data calculated from[18]

$$E_g(x,T)=(-313+1787x+444x^2-1237x^3+932x^4)+(667-1714x+760x^2)\frac{T(K)}{1000}. \tag{25}$$

The strong nonparabolicity for electrons, heavy- and light-holes state dispersions, mainly due to the admixture of Γ_8 bands and their coupling to the Γ_6 (conduction) and Γ_7 (spin-orbit) bands can be clearly observed. The spin-orbit sub-bands are not shown since they display a much weaker nonparabolicity due to their very small coupling to the valence states and to almost negligible coupling to the conduction states. These spin-orbit states are important, however, since they couple only with the light-hole branches of Γ_8 and the effect of this coupling appears as an upward shift of the lh states close to $\mathbf{k}=0$ to higher energies and as an enhancement of the minigaps between lh and hh branches at the anticrossings regions.

In Fig. 2 we show the calculated interband optical absorption, for the $Hg_{(1-x)}Cd_xTe$-$Hg_{(1-y)}Cd_yTe$ multiple quantum well with $L_z=80$ Å at a temperature of $T=145$ K. The sample has Cd concentrations $x=0.386$ in the well and $y=0.860$ in the barrier layers, respectively. We display the optical absorptions calculated with (thick lines) and without (thin lines) the contributions from excitons, given in $\alpha_{ex}(0)$, and we have chosen two values for the linewidth. The value

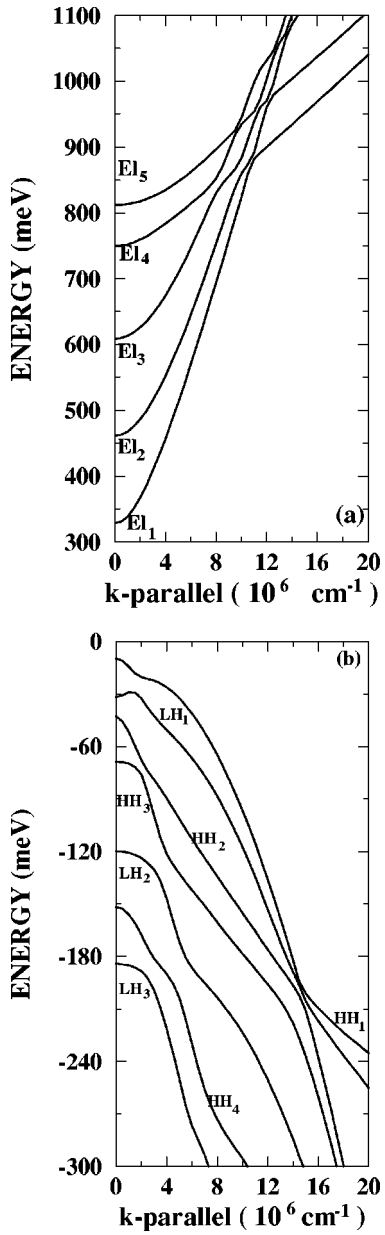

FIG. 1. Electronic band structure, for electrons (a) and heavy- and light-hole states (b), calculated for a $Hg_{(1-x)}Cd_xTe$-$Hg_{(1-y)}Cd_yTe$ MQW at temperature $T=300$ K and $L_z=100$ Å. The Cd concentrations are $x=0.27$ for the well and $y=0.85$ for barrier layers, respectively.

of 4 meV for the curves in solid lines was estimated from Eq. (22) and the 11 meV value for the two curves in dotted lines was picked for the sake of comparison. As expected, the small values for the linewidth show how much stronger are the excitonic oscillator strengths as compared to those for normal band-to-band transitions. Note that, for very small linewidths and in the limit of $T\rightarrow 0$, the optical absorption without excitons will resemble, basically, the joint density-of-states of two-dimensional systems. We also observe the ''permitted transitions'' satisfying the normal selection rules, $\Delta n=0$, however, due to the negligible value of $Q_{ij}(\mathbf{k})$ for HgCdTe quantum wells, the ''forbidden transitions'' that would be shown in the plateau regions just above the lh_{11} and hh_{22} excitonic peaks are not seen.

In Fig. 3 we present a comparison of the calculated and

TABLE I. Parameters for HgTe and CdTe taken from Refs. 12,21 The negative signs in the effective masses for the electron and light hole, in the HgTe column, refer to the ''inverted band structure'' of HgTe, with E_g negative [see Eq. (25)] and the conduction band having a p character from the Γ_8 subset of Bloch states at $\mathbf{k}=0$.

Parameters	HgTe	CdTe
m_{Γ_6} (m_0)	-0.014	0.096
$E_g(x,T)$ (meV)	see Eq. (25)	see Eq. (25)
Δ_{SO} (meV)	1080.0	951.0
$m_{\Gamma_8}(001)$ hh (m_0)	0.420	0.410
$m_{\Gamma_8}(111)$ hh (m_0)	0.530	0.530
$m_{\Gamma_8}(001)$ lh (m_0)	-0.0165	0.103
$m_{\Gamma_7}(001)$ SO (m_0)	0.102	0.280
$a(x)$ (Å)	6.461	6.481
C_{11} $(10^{11}$ dyn/cm$^2)$	5.971	6.4782
C_{12} $(10^{11}$ dyn/cm$^2)$	4.154	4.154
a_c-a_ν (meV)	3200.0	3840.0
b_ν (meV)	-1150.0	-1150.0

measured interband absorption spectra for the $Hg_{(1-x)}Cd_xTe$-$Hg_{(1-y)}Cd_yTe$ multiple quantum well with $L_z=100$ Å. The solid line is the measured spectrum and the dashed line the calculated one. There is good agreement for all the confined transitions, the calculated spectrum reproduces well both the transition energies and intensities.

Note that there is also a continuous increase of the interband absorption for energies higher than about 0.85 eV (marked by arrow 1 in Fig. 3). The sharp increase at 1.2 eV (arrow 2) is due to the barrier absorption. The enhancement of the interband absorption can be explained by an increase of the electron-hole joint density of states due to mixing of the confined and extended states near the barrier energy for

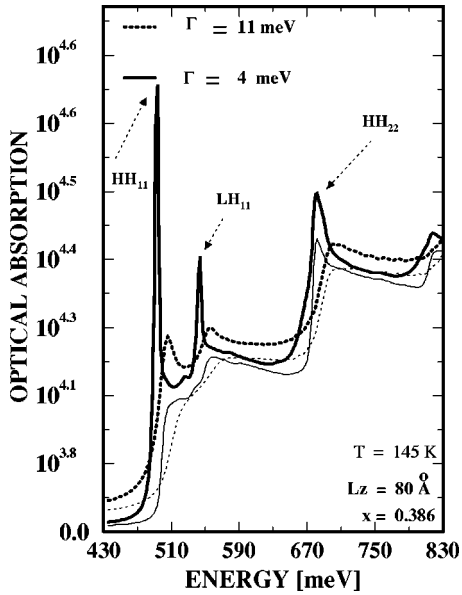

FIG. 2. Interband optical absorption for $Hg_{(1-x)}Cd_xTe$-$Hg_{(1-y)}Cd_yTe$ quantum well at $T=145$ K and $L_z=80$ Å. Small values of linewidth enhances the excitonic peaks. Only $\Delta n=0$ transitions are seen, due to small admixture in the electronic states for this material.

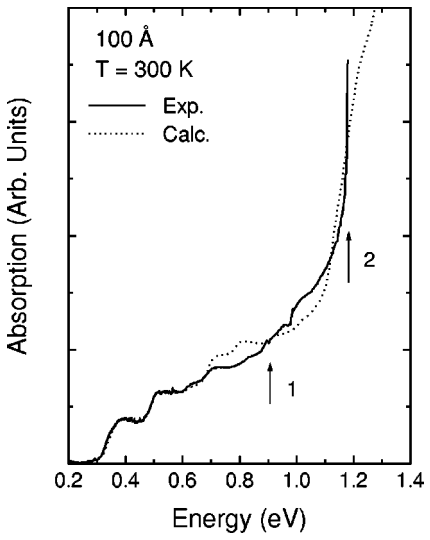

FIG. 3. Experimental (solid line) and calculated (dashed line) absorption spectra for the 100 Å HgCdTe MQW. Calculated spectra with 20 bands. The vertical arrows indicates the transitions for energies close to the barrier energy for electrons (arrow 1) and energy of the barrier layer (arrow 2).

the electrons (see Fig. 1). The band mixing near the electron barrier energy causes a rounding of the electron subbands which increases substantially the electron-hole joint density of states at these energies, about 800 meV in Fig. 1(a).

We now present the results for the photoinduced intersubband absorption in the conduction band. Figure 4 shows the calculated intersubband optical absorption for the 80 Å HgCdTe quantum wells (same sample as in Fig. 2). We considered two values for the linewidth, 8 meV in the solid line and 12 meV in the dotted line. The stronger peak (P1) is

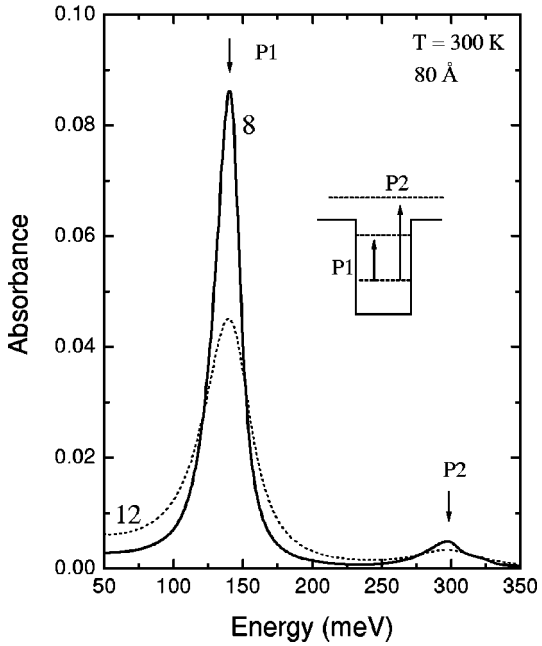

FIG. 4. Intersubband optical absorption for $Hg_{(1-x)}Cd_xTe$-$Hg_{(1-y)}Cd_yTe$ MQW at $T=145$ K and $L_z=80$ Å. Two values for the linewidth of both peaks P1 and P2, are shown. The concentrations of Cd in each layer are the same as in Fig. 2, where the well layer has ''direct band structure'' type.

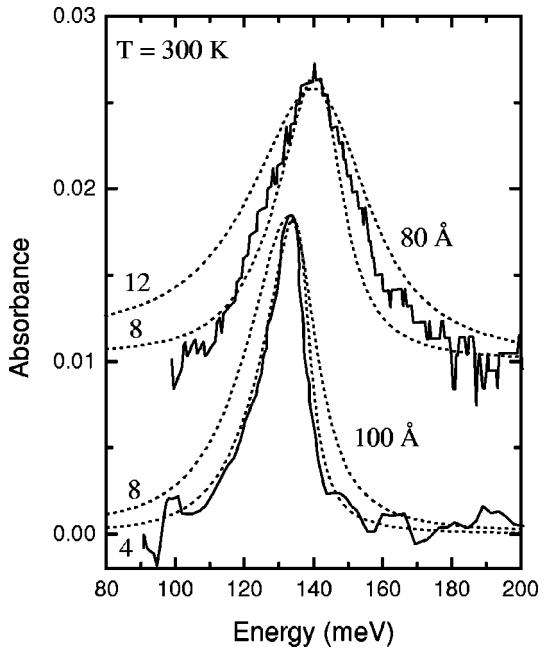

FIG. 5. Photoinduced intersubband (first electron subband to second one) for the 80 and 100 Å HgCdTe MQW at room temperature (300 K). The solid lines are the measured spectra and the dotted lines the calculated ones. The used linewidth are indicated in meV.

related to the transitions between confined states (from the first electron subband to second one) and the high-energy peak (P2) to transitions were the final states have energy above the barrier (see inset). We have used a photoexcited electron density determined from experimental measurements[9] as $N_0=1.0\times10^{10}$ and two values for Γ_{ij} for sake of comparison. It is clear that the transitions to the continuum have a much weaker oscillator strength than the transitions between localized states, due to the small overlap of the wavefunctions in the calculated $\mathbf{Q}_{ij}(\mathbf{k})$. For the same reason, they also have 3–4 orders of magnitude smaller oscillator strengths than the interband transitions obeying the $\Delta n=0$ selection rule. This is because allowed intersubband optical transitions occur between localized states with opposite parities, which determine their small oscillator strength. In fact it is expected that the intersubband oscillator strengths are of the same order of the ''forbidden transitions,'' $\Delta n>0$, in the interband transitions, as described in Sec. III B. The nonparabolicity also strongly influences the shape of these lines as well as the linewidth.[9,19,20] The asymmetric broadening to the low-energy side is due to the nonparabolicity effects. This asymmetry appears because there is a fast decrease in the intersubband transition energy as the k parallel increases (see Fig. 1).

Figure 5 shows the comparison of the calculated and measured photoinduced intersubband absorption for the 80 and 100 Å $Hg_{(1-x)}Cd_xTe$-$Hg_{(1-y)}Cd_yTe$ multiple quantum wells. The solid lines are the measured spectra and the dotted lines the calculated ones. For the 100 Å sample the calculated curve with linewidth of 4 meV reproduces very well the measured absorption. The curve with linewidth of 8 meV is broader than the experimental one. For the 80 Å sample the calculated curve with linewidth of 8 meV is close to the measured width. The curve with linewidth of 12 meV is

again broader than the experimental one. The calculated spectra reproduce well the observed asymmetric broadening to low energy in the measured intersubband transitions. Also the calculated transition energies match very well the measured values.

We should stress that both the interband and intersubband transition energies depend on the value of valence band offsets used in the band structure calculation. We could reproduce both the measured interband and intersubband spectra (Figs. 3 and 5) with the same value for the valence band offset (360 meV).

V. CONCLUSIONS

We presented measurements for the interband and intersubband absorption in HgCdTe MQW. We calculated these absorption spectra using a full 8×8 $\mathbf{k}\cdot\mathbf{p}$ Kane model to obtain the electronic structure. The interband spectrum covering the energy range from the band edge to the barrier energy shows that there is an enhancement of the absorption at energies close to the barrier energy for electrons. The calculated absorption reproduces well the confined interband transitions and predicts that this interband absorption enhancement is caused by an increase in the electron-hole joint density of states due to band mixing for confined and continuous electron states. The photoinduced electron intersubband absorption shows an asymmetric line shape to the low-energy side due to the nonparabolic bands. The calculated spectrum matches well both the line shape and transition energies. Also a value of 360 meV was determined for the valence band offset.

ACKNOWLEDGMENTS

We acknowledge financial support from CNPq, PADCT, and Fapesp.

*Present address: Universidade São Francisco, Av. São Francisco de Assis 218, 12900-000 Bragança Paulista-SP, Brazil. Electronic address: adepaula@usf.br

[1] G. Bastard, *Wave Mechanics Applied to Semiconductor Heterostructures* (Les Editions de Physique, Les Ulis, France, 1988).
[2] R. Cingolani and K. Ploog, Adv. Phys. **40**, 535 (1991).
[3] F. Szmulowicz and G. J. Brown, Appl. Phys. Lett. **66**, 1659 (1995).
[4] F. Szmulowicz and G. J. Brown, Phys. Rev. B **51**, 13 203 (1995).
[5] J. R. Meyer, C. A. Hoffman, and F. J. Bartoli, in *Narrow-gap II-VI Compounds for Optoelectronic and Electromagnetic Applications*, edited by P. Capper (Chapman Hall, London, 1997), Chap. Quantum wells and superlattices, pp. 363–400.
[6] C. L. Cesar, M. N. Islam, R. D. Feldman, R. Spitzer, R. F. Austin, A. E. DiGiovanni, J. Shah, and J. Orenstein, Appl. Phys. Lett. **54**, 745 (1989).
[7] C. L. Cesar, M. N. Islam, R. D. Feldman, R. F. Austin, D. S. Chemla, L. C. West, and A. E. DiGiovanni, Appl. Phys. Lett. **56**, 283 (1990).
[8] C. L. Cesar, M. N. Islam, C. E. Soccolich, R. D. Feldman, R. F. Austin, and K. R. German, Opt. Lett. **15**, 1147 (1990).
[9] C. R. M. de Oliveira, A. M. de Paula, C. L. Cesar, L. C. West, C. Roberts, R. D. Feldman, R. F. Austin, M. N. Islam, and G. E. Marques, Appl. Phys. Lett. **66**, 2998 (1995).
[10] T. H. Myers, J. R. Meyer, C. H. Hoffman, and L. R. Ram-Mohan, Appl. Phys. Lett. **61**, 1814 (1992).
[11] A. M. Cohen and G. E. Marques, Phys. Rev. B **41**, 10 608 (1990).
[12] G. E. Marques and A. M. Cohen, Braz. J. Phys. **24**, 230 (1994).
[13] V. A. Chitta, M. H. Degani, A. M. Cohen, and G. E. Marques, Phys. Rev. B **38**, 8533 (1998).
[14] K. H. Goetz, D. Bimberg, H. Jurgensen, J. Selders, A. V. Solomonov, G. F. Glinskii, and M. Razeghi, J. Appl. Phys. **54**, 4543 (1993).
[15] J. Hegarty and M. D. Sturge, J. Opt. Soc. Am. B **2**, 1143 (1985).
[16] *Intersubband Transitions in Quantum Wells*, edited by E. Rosencher and B. Levine (Plenum, New York, 1992).
[17] R. Q. Yang, J. M. Xu, and M. Sweeny, Phys. Rev. B **50**, 7474 (1994).
[18] *Properties of Mercury Cadmium Telluride, EMIS Datareview Series* No. 3, *INSPEC*, edited by J. C. Brice and P. Capper (Institute of Electrical Engineers, England, 1987).
[19] M. Zaluzny, Phys. Rev. B **43**, 4511 (1991).
[20] C. Sirtori, F. Capasso, J. Faist, and S. Scandolo, Phys. Rev. B **50**, 8663 (1994).
[21] *Semiconductors: Physics of II-VI and I-VII Compounds, Semimagnetic Semiconductors*, edited by O. Madelung, M. Schulz, and H. Weiss, Landolt-Börnstein, Numerical Data and Functional Relationships in Science and Technology, New Series, Vol. 17, Pt. b (Springer-Verlang, Berlin, 1982).